Chinese Journal of Chemical Engineering 77 (2025) 93–101

Contents lists available at ScienceDirect

Chinese Journal of Chemical Engineering

journal homepage: www.elsevier.com/locate/CJChE

Perspective Article

Modification mechanism of caking property of polystyrene waste using low-temperature pyrolysis and its use in coal-blending coking

Xiangchun Liu *, Ying Chen , Huan Song , Ping Cui *

Anhui Province Key Laboratory of Coal Clean Conversion & High Valued Utilization, School of Chemistry and Chemical Engineering, Anhui University of Technology, Ma'anshan 243032, China

ARTICLE INFO

Article history:
Received 24 June 2024
Received in revised form
2 September 2024
Accepted 5 September 2024
Available online 12 November 2024

Keywords:
Polystyrene
pyrolysis
Caking index
Coking property

ABSTRACT

Polystyrene (PS) waste was depolymerized using a low-temperature pyrolysis treatment (LTPT) to increase its caking index. The mechanism of caking index modification was revealed by using Fourier transform infrared spectroscopy, thermogravimetric (TG) analysis, pyrolysis-gas chromatography with mass spectrometric detection, and solid-state ^{13}C nuclear magnetic resonance spectroscopy. The crucible coal-blending coking tests were carried out using an industrial coal mixture and the treated-PS with the highest caking index (PS300) or raw PS. Some properties of the resultant cokes were also analyzed. It was demonstrated that the caking index of PS dramatically increased by LTPT; however, exceeding 300 °C did not yield any benefit. The caking index increased due to the formation of the caking components, whose molecules are medium in size, caused by LTPT. Additionally, the coke reactivity index of the coke obtained from the mixture containing PS300 decreased by 5.1% relative to that of the coke made from the mixture with PS and the coke strength after reaction index of the former increased by 7.3% compared with that of the latter, suggesting that the ratio of depolymerized PS used for coal-blending coking could increase relative to that of PS.

© 2024 Chemical Industry and Engineering Society of China, and Chemical Industry Press Co., Ltd. All rights are reserved, including those for text and data mining, AI training, and similar technologies.

1. Introduction

Global production of plastics, which are non-biodegradable, was about 400 million metric tonnes in 2022, and annual global production of plastics is predicted to twice over the following 20 years. It is expected that plastic-waste production will reach fourfold current levels in the next 20 years [1]. Plastic wastes have caused serious environmental issues [2]. Polystyrene (PS), which consists of styrene monomers, is one of main commodity plastics. PS waste accounts for approximately 10% of total plastic wastes produced annually [3].

Pyrolysis as a means of recycling PS has been extensively researched. Pyrolysis could convert PS waste into valuable chemicals, and value is recovered from PS waste. The macromolecules of PS are decomposed into relatively small molecules during pyrolysis process [4], with the formation of various hydrocarbons, which can be divided into liquid, gaseous, and solid products. Currently, studies on PS pyrolysis have primarily concentrated on the volatile products (*i.e.*, liquid and gaseous products), which are high value-added fuels and chemicals. Some liquid products can be used directly as fuels [5]. Researchers have adjusted pyrolysis conditions, *e.g.*, temperature, residence time, pressure, and reactor, to increase the yield of liquid products. It was found that pyrolysis products strongly depend on temperature. It is advised to pyrolyze PS at a temperature below 500 °C to obtain the optimum content of liquid products [5]. Additionally, some aromatics (*e.g.*, styrene, toluene, xylenes, and benzene) and a little aliphatics can be produced through PS pyrolysis [5,6]. Noteworthy, the aforementioned recycled products have practical economic benefits and can be further used as chemicals. Demirbas [7] reported that the yield of styrene obtained from PS pyrolysis increases from 56% to 64% within the temperature range of 377–477 °C and decreases with an further raise in temperature. They also detected a little amount of C2–C4 hydrocarbons. The pyrolysis mechanism of PS has been studied [6,8,9]. It can be divided into three stages: (1) oligomers are formed at low temperatures by primary homolytic breakage and intramolecular H shift; (2) styrene is produced at medium temperatures by random breakage and oligomer depolymerization; and (3) toluene, ethylbenzene, α-methylstyrene, and other

* Corresponding authors.
E-mail addresses: chunliu7@ahut.edu.cn (X. Liu), cokecp@ahut.edu.cn (P. Cui).

https://doi.org/10.1016/j.cjche.2024.09.025
1004-9541/© 2024 Chemical Industry and Engineering Society of China, and Chemical Industry Press Co., Ltd. All rights are reserved, including those for text and data mining, AI training, and similar technologies.

compounds were generated at high temperatures by secondary reactions of β-cleavage and intramolecular/intermolecular H shift. From literature review, studies of the pyrolysis mechanism of PS to quantitatively forecast the volatile-product distributions have been widely reported; however, less attention has been devoted to the use of solid product.

Currently, the shortage of coke-making coals is a factor hindering the development of the coking industry [10]. To make sensible use of coke-making coals, it is common practice in a coking plant to use a coal mixture when producing coke. PS with rich carbon and hydrogen is an alternative choice for a partial substitute of coke-making coals, and it has been demonstrated that plastic wastes can be used in commercial-scale coal-blending coking [11,12], which started in 2000 at Nippon Steel Corporation, with an initial recycling capacity of 80000 $t \cdot a^{-1}$ [13]. However, the proportion of plastic wastes used in coal-blending coking is extremely limited and typically does not exceed 3% by mass without degrading the quality of coke [14,15]; this is partly because co-carbonizing coal with plastics releases a large amount of volatile substances, which affect both caking and coking characteristics for coal. Additionally, the volatile substances released during plastic-waste carbonization lead to an increase in coking pressure, and an excessive coking pressure damages the walls of a coke oven [12]. Previous studies focused on how the blending ratio, particle size, and type of plastic wastes added affect the caking and coking characteristics for coal. Melendi *et al.* [15] reported that adding PS into a coal blend decreases coking pressure compared with adding polyolefins. The amount and temperature range of volatile substances released during pyrolysis of a plastic waste as well as the H-donor capacity of a plastic waste crucially influence the caking and coking characteristics for coal [16]. It has been demonstrated in literature that pyrolysis could break down the long polymer chains of PS into relatively small molecules with the release of volatile substances.

Using depolymerized PS in coal-blending coking has not, as far as we know, been the subject of any research. In this paper, we suggested treating PS using a low-temperature pyrolysis treatment (LTPT) to partially decompose PS into relatively small molecules. The treated-PS exhibited improved caking property in comparison with raw PS. To reveal the mechanism of LTPT improving the caking property of PS, a series of characterizations were used. Moreover, the application of the treaded-PS and raw PS in coal-blending coking was also studied. The coke reactivity (CR) toward CO_2 index, coke strength after reaction (CSR) index, and other properties of the cokes were measured. This study could offer guidelines for increasing PS content used in coal-blending coking, which could broaden coke-making coal resources and promote environmental protection.

2. Experimental

2.1. Sample

The PS waste was bought from Guangyuan Plasticization (Guangdong, China) with particle sizes less than 0.15 mm.

2.2. LTPT

PS (1 g) was pyrolyzed in a tube furnace (TL1200, Nanjing Boyuntong Instrument, China) under N_2 gas atmosphere. Fig. 1 depicts the tube furnace apparatus schematically. N_2 gas was introduced into the system at 15 $ml \cdot min^{-1}$ for 10 min to eliminate air. The experiments were conducted at 200, 250, 300, and 350 °C at 10 $°C \cdot min^{-1}$ for 40 min. The obtained solid products were labeled as PS200, PS250, PS300, and PS350, respectively. The proximate and ultimate analyses of PS, PS200, PS250, PS300, and PS350 are shown in Table 1.

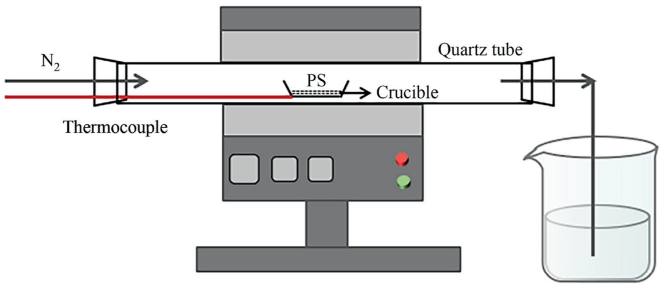

Fig. 1. Schematic of tube furnace apparatus.

2.3. Characterization

The caking index (G) tests were conducted according to Chinese Standard (GB/T5447—2014). The Supplementary materials contain a detailed description of the G measurement. The KBr method was used to record all Fourier transform infrared (FT-IR) spectra on a Nicolet 6700 spectrometer (Thermo Fisher, USA). The thermogravimetric (TG) and derivative TG (DTG) curves were measured by placing samples (approximately 9 mg) in crucibles on a thermal analyzer (STA2500 Regulus, Netzsch, Germany). The samples were heated at 10 $°C \cdot min^{-1}$ under a N_2 flow rate of 150 $ml \cdot min^{-1}$. Details of pyrolysis-gas chromatography with mass spectrometric detection (Py-GC/MS) measurements have been reported previously [17]. The Supplementary Materials contain a brief description of the Py-GC/MS measurement. An NMR-spectrometer (vnmrs600, Agilent, USA) was used to record the solid-state ^{13}C nuclear magnetic resonance (^{13}C NMR) spectra. The Raman measurements were performed on a Raman spectrometer (inVia, Renishaw, UK). The PeakFit v4.12 was used to fit all Raman spectra. The pore size distribution was determined by N_2 adsorption—desorption method at 77 K using a surface area and porosity analyzer (Micromeritics ASAP 2460, USA), and was calculated using the Barrett—Joyner—Halenda equation. Adsorbed gases were removed by pre-treatment under vacuum at 300 °C for 5 h.

2.4. Crucible coking experiment

Based on the coal-blending scheme used in a coking plant, the blending ratio used here was fat coal (20% (mass)), coking coal (40% (mass)), lean coal (7% (mass)), 1/3 coking coal (30 % (mass)), and 3% (mass) of PS or PS300. Each mixture (100 g) was placed into a crucible. After being charged into a laboratory-scale coke oven, the covered crucible was heated up to 950 °C at 3 $°C \cdot min^{-1}$ for 30 min under an inert atmosphere, which was finally cooled to room temperature. The cokes obtained were designated as C-PS and C-PS300, respectively.

Table 1
Proximate and ultimate analyses of PS and its pyrolysates (% (mass))

	Proximate analysis			Ultimate analysis (daf)				
	A_{ad}	V_{daf}	FC_{daf}	C	H	S	N	O (diff.)
PS	0	98.2	1.8	91.7	7.7	0.1	0.1	0.4
PS200	0	97.3	2.7	91.2	7.7	0.1	0.1	0.9
PS250	0	98.0	2.0	90.2	7.7	0.2	0.1	1.8
PS300	0	97.6	2.4	90.4	7.6	0.2	0.1	1.7
PS350	0	97.9	2.1	92.0	7.6	0.1	0.1	0.2

Note: diff.—difference.

2.5. Coking property

Two types of the resultant coke (20 g; 3–6 mm in size) were heated at 1100 °C for 2 h under CO_2 atmosphere with 0.5 L·min^{-1}, and the mass loss percentage following the reaction is defined as CR. The aforementioned reacted-coke (5 g) was charged into a cylinder containing 8 steel ball-bearings, which was then rotated 100 revolutions at 25 r·min^{-1}. CSR refers to the mass percentage of the reacted-coke retaining after 100 revolutions on a sieve with 1-mm apertures to the mass of the original reacted-coke.

3. Results and Discussion

3.1. Changes in G

It is frequently employed *G* to estimate the caking ability of a coal and *G* is strongly associated with its coking property [18]. Fig. 2 displays LTPT affecting the *G* of PS. From Fig. 2, the *G* showed an increasing trend below 300 °C, which decreased when the temperature further raised, suggesting that the caking ability for PS was improved by LTPT. Notably, there was an optimum temperature (*i.e.*, 300 °C), showing that a suitable degree of degradation favored the improvement of the *G* of PS. The effects of LTPT on some properties of PS were systematically studied to understand the mechanism of the increase in *G* resulted from LTPT, as presented in Section 3.2.

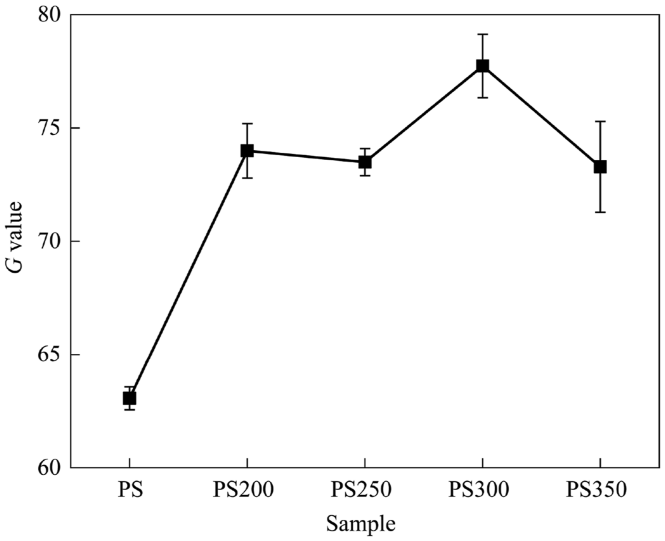

Fig. 2. Effects on caking index (*G*).

3.2. Changes in some properties

3.2.1. TG-DTG

To study how LTPT affects the pyrolysis behavior of PS, the TG and DTG curves of PS before and after treatment are presented in Fig. 3. From Fig. 3(a), the depolymerization of PS without apparent release of volatile substances occurred below 300 °C, resulting in a reduce in polymerization degree of PS [19]. McNeil *et al.* [20] stated that the molecular weight of PS decreases from 200 °C to 300 °C with slight emission of volatile substances. Fig. 3(a) also shows the main mass losses of PS and its solid pyrolysates occurred at the temperatures of 315–440 °C with negligible residues. The main mass losses are because of the emission of volatile substances resulted from the cleavage of polymer chains. Overall, PS pyrolysis occurred without significant release of water at the beginning and with minimal solid residue at the end. Notably, the mass loss increased from PS to PS300 at the same temperature; this can be attributed to that the macromolecules of PS polymer are degraded to relatively small molecules by LTPT, thereby decreasing its thermal stability.

From Fig. 3(b), the peak temperatures for PS, PS200, PS250, PS300, and PS350 were 406, 405, 407, 404, and 398 °C, respectively, and the maximum pyrolysis rate showed a decreasing trend from PS to PS350; this confirmed that LTPT could decrease the thermal stability and pyrolysis intensity of PS, which both showed a decreasing trend as the temperature increased.

3.2.2. FT-IR

Fig. 4(a) shows LTPT affecting the functional groups of PS. From Fig. 4(a), the FT-IR spectra of all samples show similar peak positions, suggesting that all samples contained similar functional groups. The peaks in the range of 3130–2990 cm^{-1}, which are caused by aromatic C—H, and the peaks at 1604, 1490, and 1448 cm^{-1}, which are assigned to aromatic C=C, suggest the presence of benzene rings [17,21,22]. The peaks in the range of 2990–2780 cm^{-1} show the presence of aliphatic C—H. Moreover, the peaks at

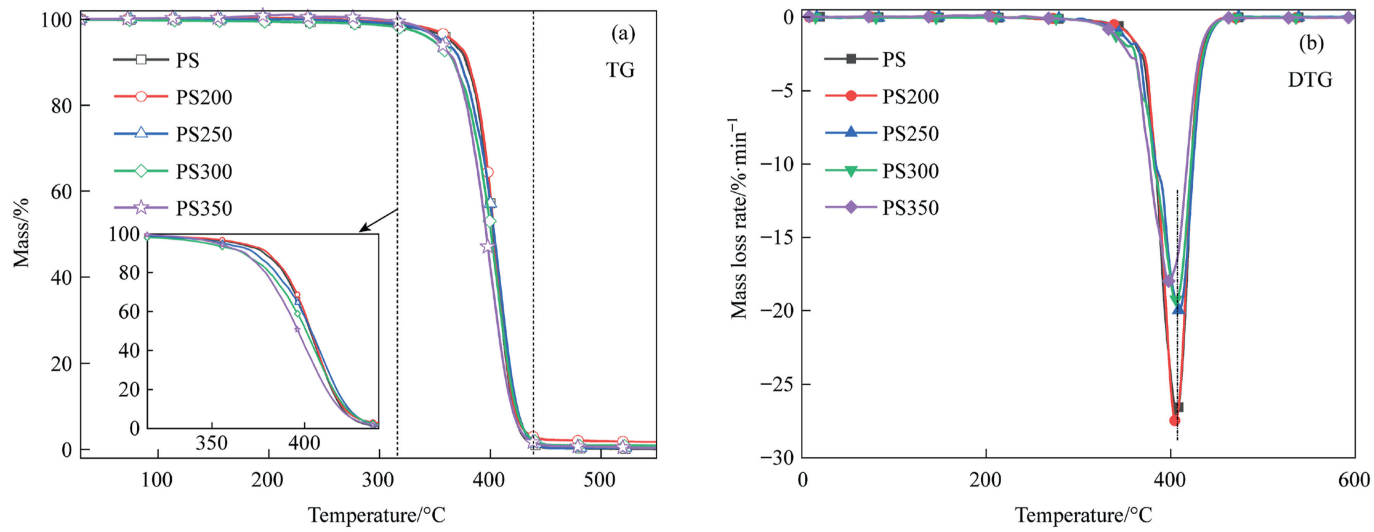

Fig. 3. TG and DTG curves of all solid products.

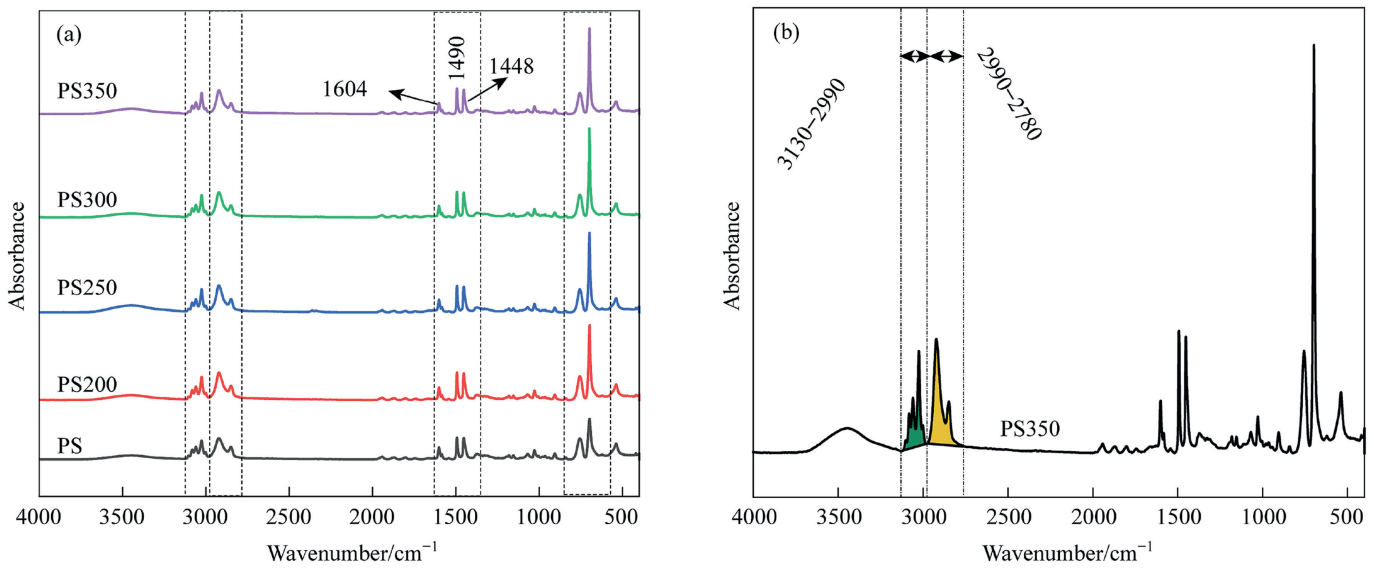

Fig. 4. (a) Effects on FT-IR spectra and (b) an example of obtaining areas ranging from 2990 to 2780 cm^{-1} and 3130–2990 cm^{-1}.

753 and 699 cm^{-1} show the presence of =C—H from mono-substituted benzene, conforming the benzene ring possessing only one substituent [23,24].

The ratio (R) of the area of 3130–2990 cm^{-1} to that of 2990–2780 cm^{-1} ($A_{3130-2990}/A_{2990-2780}$) represents the ratio of the relative content of aromatic H to that of aliphatic H; the R values for all solid products are listed in Table 2. Fig. 3(b) provides an illustration of how to get the areas of the two bands. The R increased from 0.526 for PS to 0.559 for PS350 (Table 2), suggesting that the removal of aliphatics exceeded that of aromatics. A detailed analysis of the volatile substances is presented in Section 3.2.3.

3.2.3. Py-GC/MS

The total ion chromatograms of the volatile substances of PS pyrolyzed at 200–350 °C are exhibited in Supplementary Material Fig. S1, and their components are shown in Tables S2–S5. Fig. 5 demonstrates the group-component distributions of the volatile substances of PS pyrolyzed at 200–350 °C by Py-GC/MS analysis. As seen, the majority of the volatile substances were aromatics with one or two rings (*i.e.*, monophenyl with a fatty chain and diphenyl with a fatty chain), along with small amounts of triphenyl with a fatty chain and other species (*e.g.*, aliphatics and O-, S-, and N-containing species). Similar results have also been found by others [8,25,26].

Moreover, the relative contents of monophenyl with a fatty chain in the volatile substances of PS pyrolyzed at 200–350 °C were 36.6%, 3.3%, 9.6%, and 2.5%, respectively. The relative contents of triphenyl with a fatty chain in the volatile substances of PS pyrolyzed at 200–350 °C were 57.9%, 88.4%, 84.2%, and 94.8%, respectively. It can be found that the formation of diphenyl with a fatty chain was thermodynamically favorable at relatively high temperatures. A similar result has been reported [27,28].

It is generally accepted that PS pyrolysis follows a typical free-radical mechanism, which consists of initiation, propagation, and termination. Cameron [29] claimed that PS initially decomposes *via* randomly cleaving the weak link of its polymer chain. Afterwards, various pyrolysates are generated *via* intramolecular H shift. Styrene monomer, linear dimer, trimer, toluene, cumene, ethylbenzene, α-methylstyrene, *etc.*, were detected in the volatile substances produced from PS pyrolysis [5,28,30]. The generation of monophenyl results from unzipping (end-chain β-cleavage) of the polymer chain of PS. The formation of styrene dimer is attributed to backbiting reactions and mid-chain β-cleavage at the third position [31,32]. Styrene trimer is generated through backbiting reactions and mid-chain β-cleavage at the fifth position [31]. Notably, the 1,3-H shift and mid-chain β-cleavage to produce trimer is receiving

Table 2
$A_{3130-2990}/A_{2990-2780}$ for all solid products obtained from FT-IR spectra

Sample	$A_{2990-2780}$	$A_{3130-2990}$	$R=A_{3130-2990}/A_{2990-2780}$
PS	37.20	19.55	0.526
PS200	44.28	23.44	0.529
PS250	41.60	22.05	0.530
PS300	54.27	29.96	0.552
PS350	35.21	19.68	0.559

Note: $A_{2990-2780}$ and $A_{3130-2990}$—integrated areas of bands at 2990–2780 and 3130–2990 cm^{-1}, respectively.

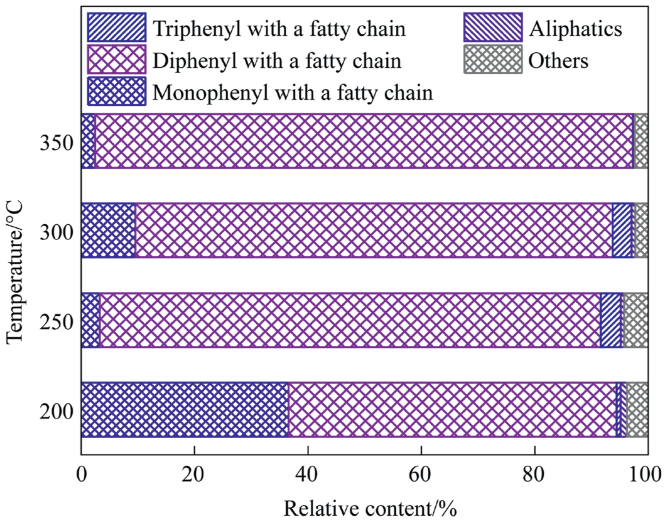

Fig. 5. Group-component distributions of volatile substances of PS pyrolyzed at 200–350 °C.

particular interest [31–33] because a high temperature is conductive to backbiting reactions, whereas the energy barrier of transition state (*i.e.*, a four-membered ring) for the 1,3-H shift is high [34]. Dimer and trimer derivatives of styrene can be formed by repolymerization [6,35]. Secondary reactions yield aliphatics [8].

3.2.4. Solid-state ^{13}C NMR

Fig. 6(a) exhibits the ^{13}C NMR spectra of PS before and after treatment to further study the impacts of LTPT on the carbon functionalities of PS. Fig. 6(a) shows that the main types of carbon in the NMR spectra were aliphatic carbons (0–53) and aromatic carbons (115–150) [36–39]. The peaks at 27, 39, 45, 127, and 145 correspond to aliphatic C(2), methylene, methine, protonated aromatic, and branched aromatic carbons, respectively [40,41], as listed in Table 3. Aliphaticity (f_{al}) and aromaticity (f_{ar}) were calculated using Eqs. (1) and (2), respectively. Table 4 displays the relative content of each carbon composition from ^{13}C NMR analysis. Fig. 6(b) shows the f_{al} and f_{ar} for all solid products.

Table 4
Relative content of each carbon composition from solid-state ^{13}C NMR analysis

Center	Symbol	Relative content/% (mol)				
		PS	PS200	PS250	PS300	PS350
0–45	$f_{al}^1+f_{al}^2+f_{al}^3$	40.21	40.02	40.19	39.36	38.71
127	f_{ar}^1	48.65	48.80	48.46	49.18	49.69
145	f_{ar}^2	11.14	11.18	11.34	11.46	11.60

$$f_{al}=f_{al}^1+f_{al}^2+f_{al}^3 \quad (1)$$

$$f_{ar}=f_{ar}^1+f_{ar}^2 \quad (2)$$

From Table 4 and Fig. 6(b), the aliphaticity decreased from 40.2% for PS to 38.7% for PS350 and the aromaticity increased from 59.8%

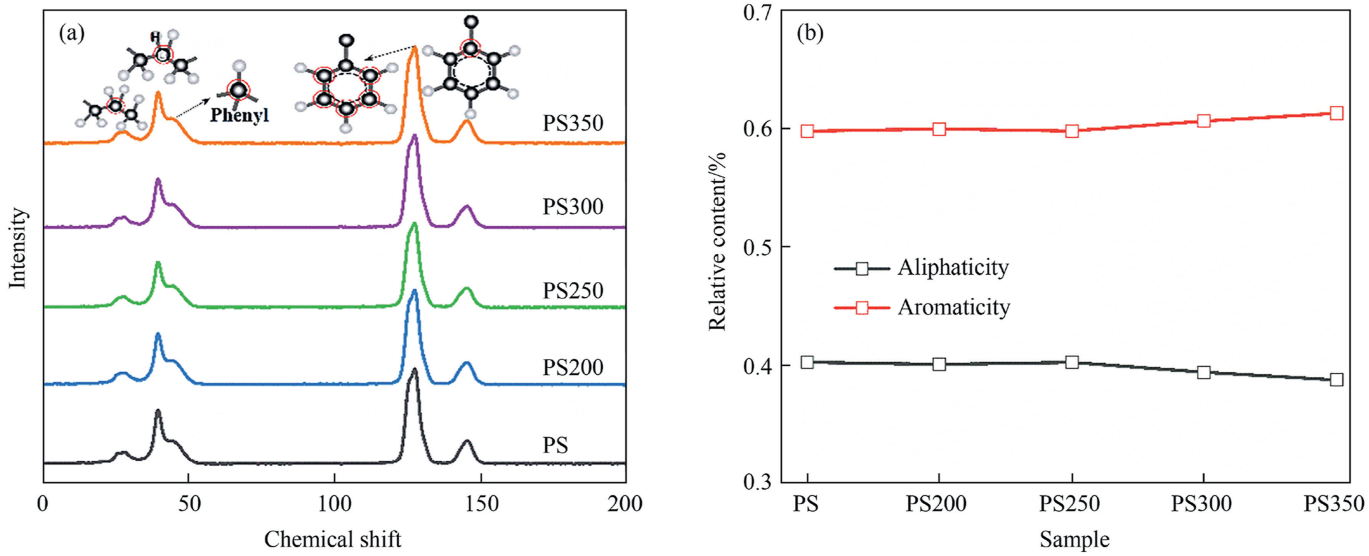

Fig. 6. Effects on (a) ^{13}C NMR spectra and (b) carbon structural parameters.

Table 3
Assignment of each peak for ^{13}C NMR analysis

	Center	Carbon functionality		Symbol
Aliphatics	27	Aliphatic C(2) carbon	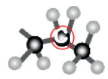	f_{al}^1
	39	Methylene carbon		f_{al}^2
	45	Methine carbon		f_{al}^3
Aromatics	127	Aromatic protonated carbon		f_{ar}^1
	145	Aromatic branched carbon	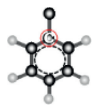	f_{ar}^2

for PS to 31.3% for PS350, which agrees well with the FT-IR result. Generally, the chain lengths of the aromatics in the volatile substances during PS pyrolysis were longer than that of styrene monomer (Tables S2–S5). In other words, the chain lengths of the removed substances were longer than that of styrene monomer; thus, the increased f_{ar} was obtained.

3.3. Modification mechanism

In accordance with the analysis of Section 3.2, we proposed a mechanism of utilizing LTPT to upgrade the caking ability of PS. PS consists of a long aliphatic chain and phenyl groups. Below 300 °C (Fig. 7(b)), monophenyl, diphenyl, triphenyl, *etc*., were produced *via* random cleavage, *β*-cleavage, unzipping, and intermolecular/intramolecular H shift reactions [6,24], which were in the form of volatile substances. Macromolecules of PS decomposed into relatively small molecules. Furthermore, the pyrolysis intensity showed a decreasing trend with increasing temperature (Fig. 4), indicating that the easily removed molecules decreased from PS200 to PS350. Additionally, the f_{ar} increased with increasing temperature. Suitable molecular weight and f_a are beneficial for the formation of caking components, whose molecules are medium in size [39]. Above 300 °C (Fig. 7(b)), the molecular weight of PS further decreased and its f_{ar} further increased as the temperature raised, which is not conducive to the caking property of PS. Consequently, the *G* reduced above 300 °C.

3.4. Coal-blending coking

The *G* of PS300 was optimum. It was therefore used for coal-blending coking. Thermal stability of coke used in a blast furnace is frequently assessed using CR and CSR [42]. It is widely acknowledged that coke with high CSR and low CR possesses a high quality [43] because high CSR and low CR mean coke has a high stability when used in a blast furnace. The CR and CSR indices of C-PS and C-PS300 are shown in Fig. 8.

From Fig. 8, the CR index of C-PS300 was 40.0%, which decreased by 5.1% relative to that of C-PS. Moreover, the CSR index of C-PS300 increased by 7.3% compared with that of C-PS, suggesting that the thermal stability of C-PS300 was higher than that of C-PS and LTPT could increase the ratio of PS used for coal-blending coking. In other words, the ratio of depolymerized PS used for coal-blending coking increased compared with that of PS. The existence of an optimum *G* indicates that depolymerizing PS to a suitable degree could maximize the content of PS used for coal-blending coking.

To reveal the reasons for the variations of the CR and CSR indices for C-PS and C-PS300, their Raman spectra, pore distributions, and

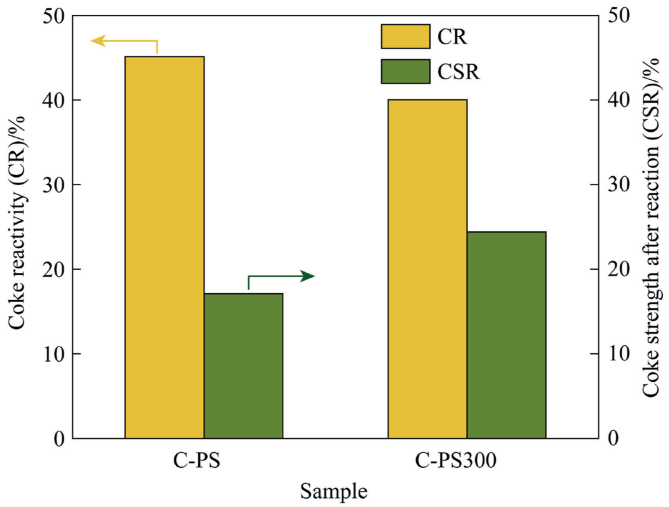

Fig. 8. CR and CSR indices for C-PS and C-PS300.

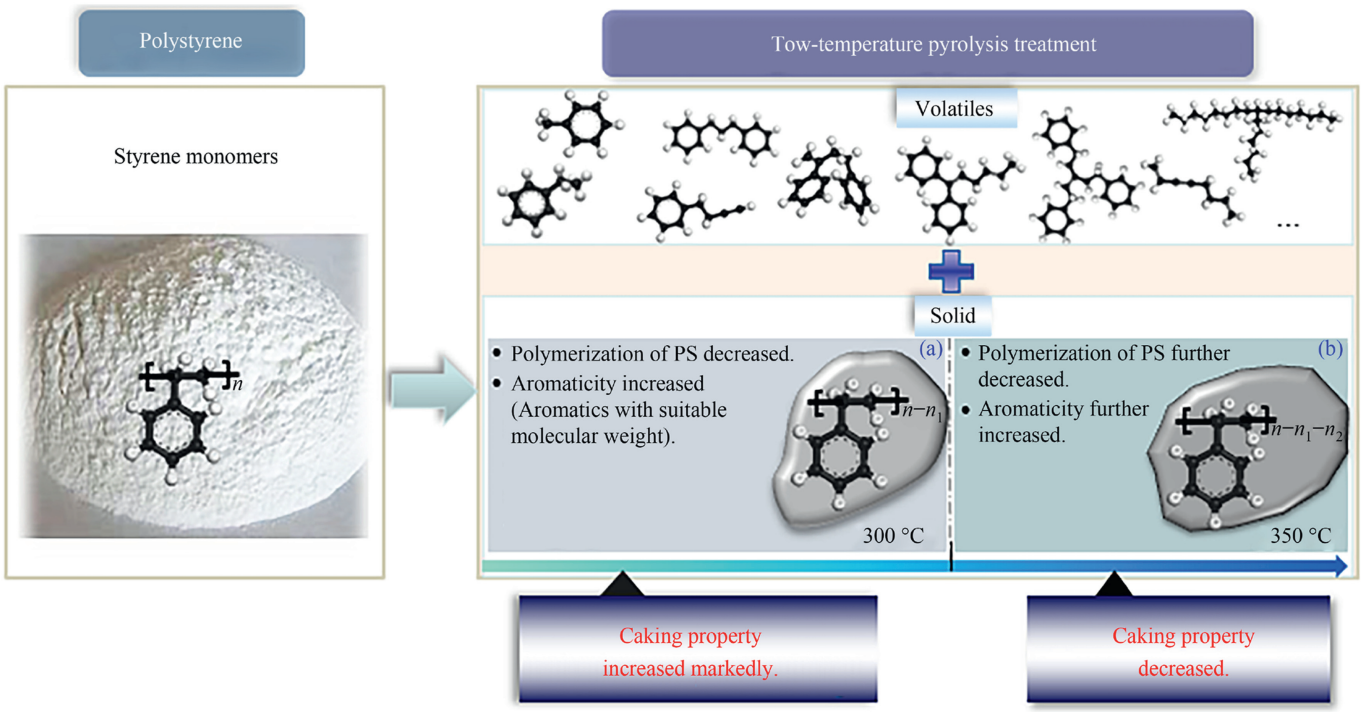

Fig. 7. A mechanism of utilizing LTPT to upgrade the caking index of PS.

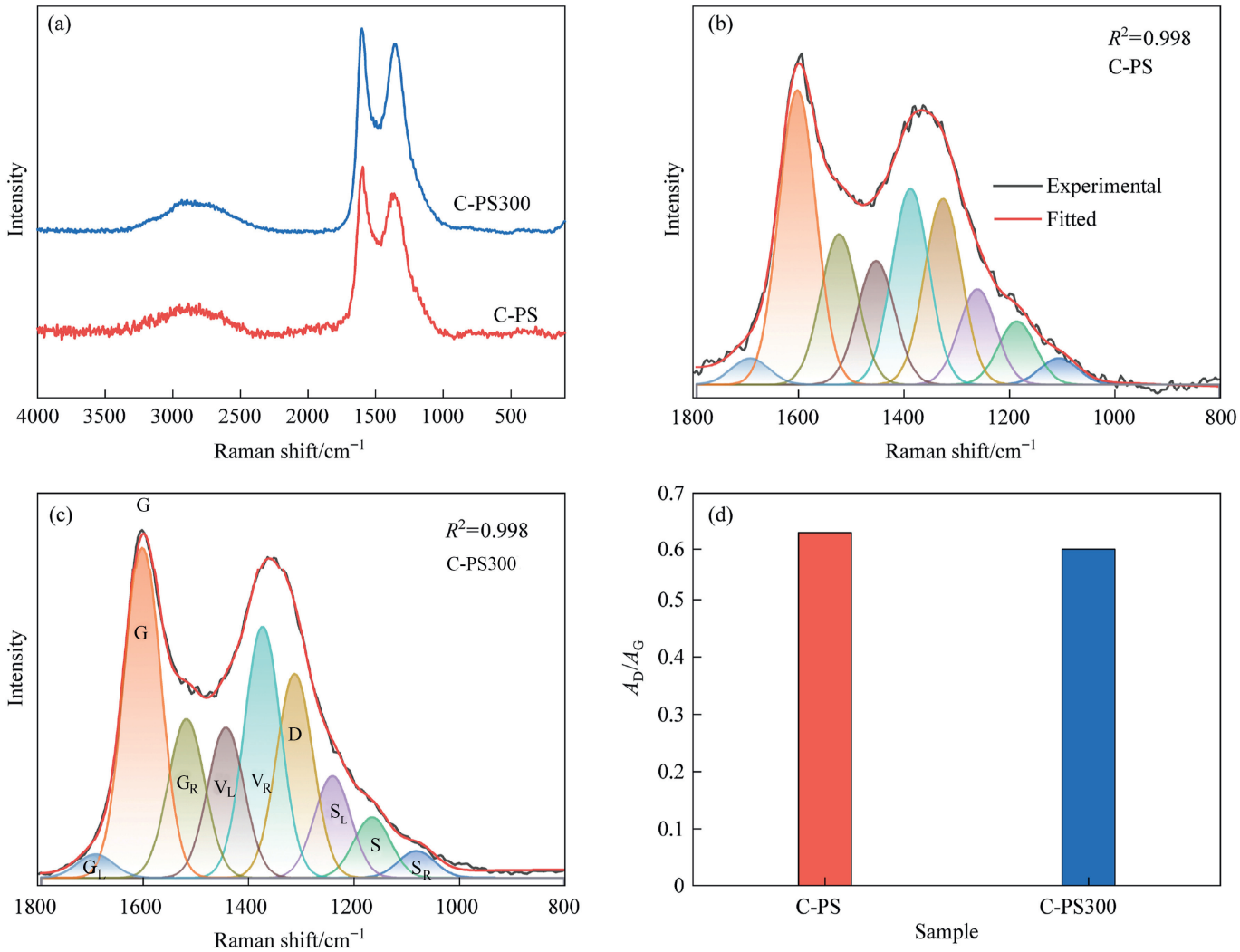

Fig. 9. (a) Raman spectra, (b, c) curve-fitted Raman spectra, and (d) A_D/A_G for C-PS and C-PS300.

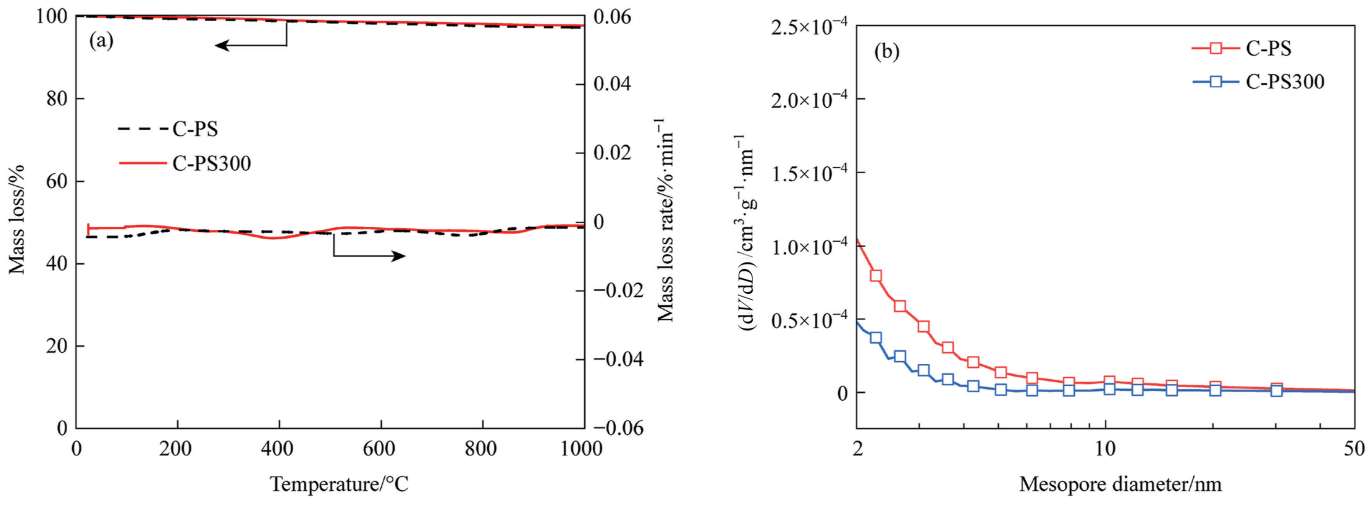

Fig. 10. (a) TG-DTG curves and (b) pore size distributions for C-PS and C-PS300.

TG-DTG curves were measured (Figs. 9 and 10). Curve-fitting the Raman spectra between 1800 and 800 cm^{-1} can quantitatively study the changes in disordered degree, as presented in Fig. 9(b) and (c). The assignment of each curve-fitted peak for the Raman spectra is listed in Table S6. Fig. 9(d) exhibits the area ratios (A_D/A_G) of the curve-fitted D peak to the curve-fitted G peak for C-PS and C-PS300.

From Fig. 9(d), the A_D/A_G value of C-PS300 was 0.60, which was lower than that of C-PS (0.63), suggesting that C-PS300 was more ordered than C-PS, leading to an increase in the ability to resist thermal damage [44]. The TG result showed that the final mass losses of C-PS300 and C-PS were 2.2% and 2.7%, respectively, suggesting the content of the volatile substances released from C-PS300 pyrolysis was lower than that released from C-PS pyrolysis; therefore, C-PS possessed a bigger pore volume than C-PS300 (Fig. 10(b)), which is favorable for the transport of reactants and products. As a result, the CR of C-PS300 was lower than that of C-PS (Fig. 8). In summary, the thermal stability of C-PS300 was higher than that of C-PS because C-PS300 was produced from the blending including PS300. PS300 was prepared using LTPT, and some easily released volatile substances were removed during LTPT process; therefore, the content of volatile substances of PS300 is relatively low.

4. Conclusions

LTPT could modify of the caking and coking characteristics of PS, and 300 °C was the optimum temperature. Based on the FT-IR, TG, Py-GC/MS and solid-state ^{13}C NMR data, we suggested an enhancement mechanism of the caking ability for PS, which is triggered by LTPT. Below 300 °C, the molecular weight of PS decreased and its f_a increased as the temperature increased. The *G* of PS increased substantially as a result of the increased yield of medium-sized-molecular-weight caking components. PS350 had a lower *G* than PS300. The molecular weight of PS300 was higher than that of PS350 and the f_a of the former was lower than that of the latter. The *G* of PS350 decreased relative to that of PS300 because the decreased molecular weight and increased f_a, which suggest that the content of medium-sized-molecular-weight caking components in PS350 decreased relative to those in PS300. Moreover, the CR of C-PS300 decreased by 5.1% compared with that of C-PS. The CSR of C-PS300 increased by 7.3% in comparison with that of C-PS. Overall, it can be concluded the LTPT could increase the proportion of PS used for coal-blending coking.

CRediT Authorship Contribution Statement

Xiangchun Liu: Writing – original draft, Supervision, Funding acquisition. Ying Chen: Investigation, Formal analysis. Huan Song: Investigation, Data curation. Ping Cui: Project administration, Funding acquisition.

Declaration of Competing Interest

The authors declare that they have no known competing financial interests or personal relationships that could have appeared to influence the work reported in this paper.

Acknowledgements

This work was supported by the National Natural Science Foundation of China (22308006 and 22278001) and the Natural Science Foundation of Anhui Provincial Education Department (KJ2021A0407).

Supplementary Material

Supplementary data to this article can be found online at https://doi.org/10.1016/j.cjche.2024.09.025.

References

[1] P.A. Athulya, N. Chandrasekaran, Interactions of natural colloids with microplastics in aquatic environment and its impact on FTIR characterization of polyethylene and polystyrene microplastics, *J. Mol. Liq.* 369 (2023) 120950.
[2] L. Olazar, J.F. Saldarriaga, G. Lopez, L. Santamaria, M. Amutio, M. Olazar, M. Artetxe, Insight into the joint valorization of CO_2 and waste plastics by pyrolysis and in line dry reforming for syngas production, *Fuel Process. Technol.* 253 (2024) 108024.
[3] A.M. Gonzalez-Aguilar, V. Pérez-García, J.M. Riesco-Ávila, A thermo-catalytic pyrolysis of polystyrene waste review: a systematic, statistical, and bibliometric approach, *Polymers* 15 (6) (2023) 1582.
[4] Z.C. Jin, L.J. Yin, D.Z. Chen, Y.J. Jia, J. Yuan, Y.Y. Hu, Co-pyrolysis characteristics of typical components of waste plastics in a falling film pyrolysis reactor, *Chin. J. Chem. Eng.* 26 (10) (2018) 2176–2184.
[5] I.M. Maafa, Pyrolysis of polystyrene waste: a review, *Polymers* 13 (2) (2021) 225.
[6] K.B. Park, Y.S. Jeong, B. Guzelciftci, J.S. Kim, Two-stage pyrolysis of polystyrene: pyrolysis oil as a source of fuels or benzene, toluene, ethylbenzene, and xylenes, *Appl. Energy* 259 (2020) 114240.
[7] A. Demirbas, Pyrolysis of municipal plastic wastes for recovery of gasoline-range hydrocarbons, *J. Anal. Appl. Pyrolysis* 72 (1) (2004) 97–102.
[8] M. Artetxe, G. Lopez, M. Amutio, I. Barbarias, A. Arregi, R. Aguado, J. Bilbao, M. Olazar, Styrene recovery from polystyrene by flash pyrolysis in a conical spouted bed reactor, *Waste Manag.* 45 (2015) 126–133.
[9] G. Audisio, F. Bertini, Molecular weight and pyrolysis products distribution of polymers I. Polystyrene, *J. Anal. Appl. Pyrolysis* 24 (1) (1992) 61–74.
[10] Y.F. Shen, Y.F. Hu, M.J. Wang, W.R. Bao, L.P. Chang, K.C. Xie, Speciation and thermal transformation of sulfur forms in high-sulfur coal and its utilization in coal-blending coking process: a review, *Chin. J. Chem. Eng.* 35 (2021) 70–82.
[11] S. Nomura, Recent developments in cokemaking technologies in Japan, Fuel Process, *Technol.* 159 (2017) 1–8.
[12] S. Nomura, K. Kato, The effect of plastic size on coke quality and coking pressure in the co-carbonization of coal/plastic in coke oven, *Fuel* 85 (1) (2006) 47–56.
[13] M.A. Diez, R. Alvarez, Advances in the recycling of plastic wastes for metallurgical coke production, *J. Mater. Cycles Waste Manag.* 15 (3) (2013) 247–255.
[14] X.X. Wang, J.W. Mu, Q.D. Zhu, Application of waste plastics in iron and steel industry, *Ind. Heat.* 50 (2021) 59–64.
[15] S. Melendi, M.A. Diez, R. Alvarez, C. Barriocanal, Relevance of the composition of municipal plastic wastes for metallurgical coke production, *Fuel* 90 (4) (2011) 1431–1438.
[16] M.A. Díez, C. Barriocanal, R. Álvarez, Plastic wastes as modifiers of the thermoplasticity of coal, *Energy Fuel.* 19 (6) (2005) 2304–2316.
[17] X.C. Liu, G.Q. Li, H.Y. Zhao, Y.G. Ye, R.L. Xie, Z.G. Zhao, Z. Lei, P. Cui, Changes in caking properties of caking bituminous coals during low-temperature pyrolysis process, *Fuel* 321 (2022) 124023.
[18] X. Li, Z.H. Qin, L.H. Bu, Z. Yang, C.Y. Shen, Structural analysis of functional group and mechanism investigation of caking property of coking coal, *J. Fuel Chem. Technol.* 44 (4) (2016) 385–393.
[19] M. Guaita, O. Chiantore, L. Costa, Changes in degree of polymerization in the thermal degradation of polystyrene, *Polym. Degrad. Stabil.* 12 (4) (1985) 315–332.
[20] I.C. McNeill, M. Zulfiqar, T. Kousar, A detailed investigation of the products of the thermal degradation of polystyrene, *Polym. Degrad. Stabil.* 28 (2) (1990) 131–151.
[21] K.B. Park, J.S. Kim, Pyrolysis products from various types of plastics using TG-FTIR at different reaction temperatures, *J. Anal. Appl. Pyrolysis* 171 (2023) 105983.
[22] X.C. Liu, H. Song, K.S. Han, J. Hu, Z.G. Zhao, P. Cui, Insight into low-temperature co-pyrolysis of Qinglongshan lean coal with organic matter in Huadian oil shale, *Energy* 285 (2023) 128678.
[23] J.F. Fang, Y.M. Xuan, Q. Li, Preparation of polystyrene spheres in different particle sizes and assembly of the PS colloidal crystals, *Sci. China Technol. Sci.* 53 (11) (2010) 3088–3093.
[24] J.B. Zhou, Y. Qiao, W.X. Wang, E.W. Leng, J.C. Huang, Y. Yu, M.H. Xu, Formation of styrene monomer, dimer and trimer in the primary volatiles produced from polystyrene pyrolysis in a wire-mesh reactor, *Fuel* 182 (2016) 333–339.
[25] J. Nisar, G. Ali, A. Shah, M. Iqbal, R. Ali Khan, Sirajuddin, F. Anwar, R. Ullah, M. S. Akhter, Fuel production from waste polystyrene *via* pyrolysis: kinetics and products distribution, *Waste Manag.* 88 (2019) 236–247.
[26] D.S. Achilias, I. Kanellopoulou, P. Megalokonomos, E. Antonakou, A.A. Lappas, Chemical recycling of polystyrene by pyrolysis: potential use of the liquid product for the reproduction of polymer, *Macromol. Mater. Eng.* 292 (8) (2007) 923–934.
[27] J.K. Koo, S.W. Kim, Y.H. Seo, Characterization of aromatic hydrocarbon formation from pyrolysis of polyethylene-polystyrene mixtures, *Resour. Conserv. Recycl.* 5 (4) (1991) 365–382.

[28] J.A. Onwudili, N. Insura, P.T. Williams, Composition of products from the pyrolysis of polyethylene and polystyrene in a closed batch reactor: effects of temperature and residence time, *J. Anal. Appl. Pyrolysis* 86 (2) (2009) 293–303.
[29] G.G. Cameron, Mechanism of volatile production during pyrolysis of polystyrene, *Makromol. Chem.* 100 (1) (1967) 255–261.
[30] M. Yang, Y. Shibasaki, Mechanisms of thermal degradation of polystyrene, polymethacrylonitrile, and their copolymers on flash pyrolysis, *J. Polym. Sci. Polym. Chem.* 36 (13) (1998) 2315–2330.
[31] S.E. Levine, L.J. Broadbelt, Reaction pathways to dimer in polystyrene pyrolysis: a mechanistic modeling study, *Polym. Degrad. Stabil.* 93 (5) (2008) 941–951.
[32] T.M. Kruse, O.S. Woo, H.W. Wong, S.S. Khan, L.J. Broadbelt, Mechanistic modeling of polymer degradation: a comprehensive study of polystyrene, *Macromolecules* 35 (20) (2002) 7830–7844.
[33] T.M. Kruse, S.E. Levine, H.W. Wong, E. Duoss, A.H. Lebovitz, J.M. Torkelson, L.J. Broadbelt, Binary mixture pyrolysis of polypropylene and polystyrene: a modeling and experimental study, *J. Anal. Appl. Pyrolysis* 73 (2) (2005) 342–354.
[34] J. Pfaendtner, X.R. Yu, L.J. Broadbelt, Quantum chemical investigation of low-temperature intramolecular hydrogen transfer reactions of hydrocarbons, *J. Phys. Chem. A* 110 (37) (2006) 10863–10871.
[35] D.K. Ojha, R. Vinu, Resource recovery *via* catalytic fast pyrolysis of polystyrene using zeolites, *J. Anal. Appl. Pyrolysis* 113 (2015) 349–359.
[36] L.H. Hou, W.J. Ma, X. Luo, S.Z. Tao, P. Guan, J.Z. Liu, Chemical structure changes of lacustrine Type-II kerogen under semi-open pyrolysis as investigated by solid-state ^{13}C NMR and FT-IR spectroscopy, *Mar. Petrol. Geol.* 116 (2020) 104348.
[37] W. Li, Y.M. Zhu, Structural characteristics of coal vitrinite during pyrolysis, *Energy Fuel.* 28 (6) (2014) 3645–3654.
[38] Q. Wang, Y.C. Hou, W.Z. Wu, Q. Liu, Z.Y. Liu, The structural characteristics of kerogens in oil shale with different density grades, *Fuel* 219 (2018) 151–158.
[39] X.C. Liu, G.Q. Li, H.Y. Zhao, F. Cheng, R.L. Xie, Z.G. Zhao, P. Cui, Upgrading deashed Huadian oil shale using low-temperature pyrolysis treatment and its application in coal-blending coking, *Fuel Process. Technol.* 223 (2021) 106994.
[40] M.A. Fichera, U. Braun, B. Schartel, H. Sturm, U. Knoll, C. Jäger, Solid-state NMR investigations of the pyrolysis and thermo-oxidative decomposition products of a polystyrene/red phosphorus/magnesium hydroxide system, *J. Anal. Appl. Pyrolysis* 78 (2) (2007) 378–386.
[41] R.H. Still, O.A. Peters, Vacuum pyrolysis of polystyrene oligomers, *J. Appl. Polym. Sci.* 50 (6) (1993) 989–994.
[42] A.M. Fernández, C. Barriocanal, S. Gupta, D. French, Effect of blending carbon-bearing waste with coal on mineralogy and reactivity of cokes, *Energy Fuel.* 28 (1) (2014) 291–298.
[43] M.A. Díez, R. Alvarez, C. Barriocanal, Coal for metallurgical coke production: predictions of coke quality and future requirements for cokemaking, *Int. J. Coal Geol.* 50 (1–4) (2002) 389–412.
[44] S. Nomura, K. Kato, T. Nakagawa, I. Komaki, The effect of plastic addition on coal caking properties during carbonization, *Fuel* 82 (14) (2003) 1775–1782.